Electron acceleration and trapping by an oblique shock wave

Naoki Bessho and Yukiharu Ohsawa
Department of Physics, Nagoya University, Nagoya 464-8602, Japan

(Received 21 August 2001; accepted 19 December 2001)

Electron acceleration to ultrarelativistic energies by an oblique magnetosonic shock wave is studied. First, the maximum electron energy is analytically obtained with new simple calculations. The physical mechanism is also discussed in detail. In the wave frame, electrons reflected near the end of the main pulse region, which will be trapped, gain energy from the electric potential and constant electric field E_{y0} perpendicular to the external magnetic field. For certain plasma parameters, these electrons can move a long distance in the direction of E_{y0} and obtain a great amount of energy from E_{y0}. It is argued that the trapped electrons can hardly escape from the shock wave. Next, one-dimensional, relativistic, particle simulations are carried out. Theoretical estimates such as the maximum electron energy are found to be in good agreement with the simulations. Simulations also show that the number of trapped electrons continually increases with time. © *2002 American Institute of Physics.* [DOI: 10.1063/1.1453473]

I. INTRODUCTION

High-energy electrons are often produced in astrophysical plasmas. For instance, in solar flares, electrons are accelerated to several tens of megaelectronvolts within a few seconds.[1–4] (For the ions, see Ref. 5.) Recent x-ray and gamma-ray observations of supernova remnants showed that electrons are accelerated to ~ 100 TeV.[6–9] Ultrarelativistic electrons are also produced in binary systems[10,11] and active galactic nuclei.[12–16]

The particle acceleration has been intensively studied by particle simulations as well as by theory[17–25] and experiments.[1–16] (For the research of plasma-based accelerators, see Ref. 26, and references therein.) Particle simulations have revealed that a large-amplitude magnetosonic wave with coherent structure can accelerate particles, i.e., hydrogen ions,[27–39] heavy ions,[40,41] and electrons,[42–44] through various mechanisms.

The electron acceleration to ultrarelativistic energies can occur in a shock wave propagating obliquely to a magnetic field with $\omega_{ce}/\omega_{pe} \gtrsim 1$, where ω_{ce} and ω_{pe} are the electron cyclotron and plasma frequencies, respectively.[42–44] In such a shock wave, some electrons can be reflected near the end of the main pulse region. The reflection is caused by a potential dip formed there; the dip can sometimes be generated by small-amplitude fluctuations of electromagnetic fields. (More precisely, transverse electric fields as well as the potential play some role in the electron reflection.) The reflected electrons are then trapped; they move back and forth in the shock wave and their kinetic energies oscillate. Their energies take their maximum values at the position of the maximum potential, $x = x_m$; here, we assume that the shock wave propagates in the x direction in an external magnetic field in the (x,z) plane. In the wave frame, where constant electric field E_{y0} appears, we see that the reflected electrons gain energy from E_{y0} and the potential φ as they move from the reflection point to x_m.

For passing electrons, on the other hand, the energy increase by E_{y0} and that by φ almost cancel. Hence, the kinetic energy of a passing electron dose not change much when it passes through the shock wave.

In Ref. 44, it was attempted to theoretically obtain the maximum energy of electrons. The derivation was, however, lengthy, and the final set of equations giving the maximum energy was complicated.

In this paper, we obtain the maximum electron energy in a different manner. It will be found that the derivation and the final expression are much simpler. Furthermore, we can give clear physical meanings to the calculations. It is shown that it takes long periods of time for reflected electrons to move from the reflection point to the point x_m, during which they travel a long distance in the y direction and gain a great amount of energy from the electric field E_{y0}. For certain plasma parameters, this period can be quite long, and hence the maximum electron energy can be extremely large. On the other hand, the energy gain from the electric potential φ is independent of this period. These theoretical calculations and physical pictures are given in Sec. II. In Sec. III, we discuss the reflection mechanism. Once an electron is reflected near the end of the main pulse, then it will be reflected there again even if the potential dip disappears at the location where the first reflection took place. This suggests that the number of trapped electrons increases with time. In Sec. IV, we investigate the shock propagation and electron acceleration, using a one-dimensional (one space coordinate and three velocity components), relativistic, electromagnetic particle simulation code with full ion and electron dynamics. It is shown that the theoretically obtained maximum electron energy agrees fairly well with the simulation result. We also show that the number of trapped electrons continually grows. In Sec. V, we summarize our work.

This mechanism could produce ultrarelativistic electrons in the coronal magnetic tubes in solar flares. The value of ω_{ce}/ω_{pe} becomes ~ 3 for plasmas with, for instance, the magnetic field strength $B \sim 10^3$ G and the density $n \sim 10^{10}$ cm^{-3}, or with $B \sim 10^2$ G and $n \sim 10^8$ cm^{-3}. These

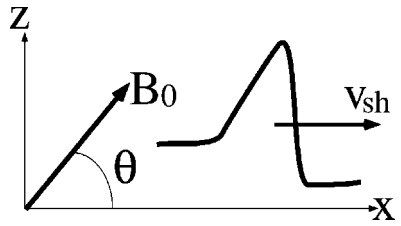

FIG. 1. Geometry of magnetic field and shock wave.

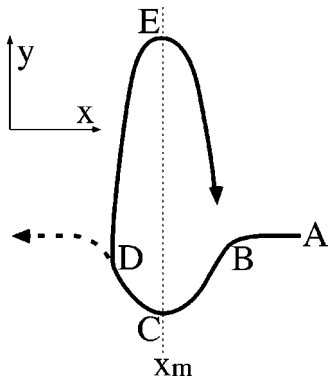

FIG. 2. Schematic diagram of guiding-center motion projected on the x,y plane. Point C and point E are on the x position of the maximum potential. The dotted line shows the orbit of a passing electron.

parameters would be found in the solar magnetic tubes. If large-amplitude magnetosonic waves are excited in such a plasma in association with solar flares, they would accelerate electrons to ultrarelativistic energies.

II. DERIVATION OF THE MAXIMUM ELECTRON ENERGY

We derive the maximum electron energy in an oblique shock wave. In the analysis, we also try to draw a clear physical picture of the electron acceleration, by carefully examining the meanings of the calculations.

A. Fundamental relations

We consider a magnetosonic shock wave propagating in the x direction ($\partial/\partial y=\partial/\partial z=0$) with a speed $v_{\rm sh}$ in an external magnetic field $\mathbf{B}_0$ in the (x,z) plane. The geometry is shown in Fig. 1; the angle between the x axis and the external magnetic field, θ, is the shock propagation angle. Then, the x component of the magnetic field is constant, $B_x=B_{x0}$. The other components B_y and B_z are functions of x, and in the pulse region B_y as well as B_z can have finite values. In the wave frame where the time derivatives are zero ($\partial/\partial t=0$), the electric field in the y direction is constant, $E_y=E_{y0}$, and E_z is zero. Hence, we have $\mathbf{B}=(B_{x0},B_y,B_z)$ and $\mathbf{E}=(E_x,E_{y0},0)$.

In such circumstances, an oblique shock wave has a positive electric potential $\varphi(x)$. The quantities φ, B_z, and density n have similar profiles.[43–46] On the other hand, E_x and B_y are proportional to the x derivatives of these quantities; for instance, $E_x=-\partial\varphi/\partial x$. These relations among the quantities are analytically obtained for small-amplitude waves.[45,46] Simulations show that these relations are also roughly satisfied for large-amplitude waves.[43,44]

The velocity of the guiding-center position of an electron, $\mathbf{v}_g$, may be written as

$$\mathbf{v}_g=\mathbf{v}_d+(\mathbf{B}/B)v_\parallel, \tag{1}$$

with $\mathbf{v}_d$ the drift velocity and $v_\parallel$ the velocity parallel to $\mathbf{B}$. If we neglect ∇B-drift (and other unimportant drifts), the x, y, and z components of $\mathbf{v}_g$ are given as

$$v_{gx}=\frac{cE_{y0}B_z}{B^2}+v_\parallel\frac{B_{x0}}{B}, \tag{2}$$

$$v_{gy}=-\frac{cE_xB_z}{B^2}+v_\parallel\frac{B_y}{B}, \tag{3}$$

$$v_{gz}=c\frac{E_xB_y-E_{y0}B_{x0}}{B^2}+v_\parallel\frac{B_z}{B}, \tag{4}$$

in the wave frame, where c is the speed of light.

In the far upstream region, the z component of the velocity averaged over all the electrons in a small volume element is zero, $\langle v_{gz0}\rangle=0$; the subscript 0 refers to the quantities in the far upstream region. Then, from Eq. (4), we have the average parallel velocity

$$\langle v_{\parallel 0}\rangle=\frac{cE_{y0}}{B_0}\frac{B_{x0}}{B_{z0}}. \tag{5}$$

Also, using the relation $\langle v_{gx0}\rangle=-v_{\rm sh}$, we find the relation between E_{y0} and the shock speed $v_{\rm sh}$ as

$$E_{y0}=-v_{\rm sh}B_{z0}/c. \tag{6}$$

For the definiteness, we assume that B_{x0}, B_{z0}, and $v_{\rm sh}$ are all positive; thus $E_{y0}<0$.

B. Estimate of the maximum electron energy

From the relativistic equation of motion for an electron particle,

$$m_e\frac{{\rm d}(\gamma\mathbf{v})}{{\rm d}t}=-e\left(\mathbf{E}+\frac{\mathbf{v}\times\mathbf{B}}{c}\right), \tag{7}$$

where γ is the Lorentz factor, we have the energy conservation equation in the wave frame,

$$m_ec^2(\gamma-\gamma_0)=e(\varphi-\varphi_0)-eE_{y0}\int v_y{\rm d}t. \tag{8}$$

Here, we have used the relations $E_z=0$ and $v_x{\rm d}t={\rm d}x$. We show in Fig. 2 a schematic diagram of guiding-center orbit projected on the (x,y) plane; an electron is reflected at point D. Point C and point E are on the peak of φ; hence, $x_C=x_E=x_m$, where x_m designates the x position at which φ, B_z, and n take their maximum values. The electric field E_x is positive in the region $x>x_m$ and is negative in $x<x_m$. Substituting the guiding-center velocity, Eqs. (2) and (3), in Eq. (8), we find the increase in the kinetic energy (for the guiding-center motion) from point B to point C as

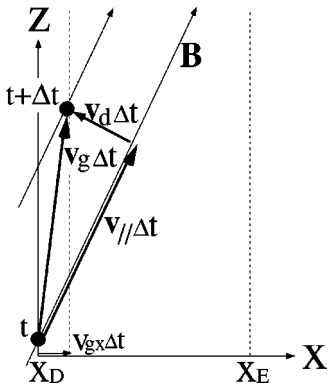

FIG. 3. Schematic diagram of guiding-center motion in the x,z plane. The two dots show particle positions at time t and $t+\Delta$. When $v_\parallel$ is positive, the x components of drift and parallel motions can almost cancel; thus, v_{gx} is small. The drift v_{dx} is proportional to E_{y0}.

$$K_{\mathrm{BC}}=e(\varphi_{\mathrm{C}}-\varphi_{\mathrm{B}})+eE_{y0}\int_{\mathrm{B}}^{\mathrm{C}}\mathrm{d}x\,\frac{E_x}{E_{y0}+(v_\parallel/c)(BB_{x0}/B_z)}$$
$$-eE_{y0}\int_{\mathrm{B}}^{\mathrm{C}}\mathrm{d}t\,\frac{v_\parallel B_y}{B}. \tag{9}$$

The first term on the right-hand side shows the energy change by the potential difference. The second and third terms represent the work done by the constant electric field E_{y0}; the former is due to the $E_x\times B_z$ drift and the latter is due to the parallel component of **v**. If an electron moves with a velocity nearly equal to the fluid velocity, then $v_\parallel$ would be negative, as suggested by Eq. (5). The denominator in the second term therefore cannot be close to zero (we recall that E_{y0} is negative). Since the denominator is proportional to the guiding-center velocity v_{gx}, this means that the electron moves quickly from point B to point C. We have a similar equation for K_{CD}.

The energy increase from point B to point E may be given as

$$K_{\mathrm{BE}}=K_{\mathrm{BC}}+K_{\mathrm{CD}}+e(\varphi_{\mathrm{E}}-\varphi_{\mathrm{D}})$$
$$+eE_{y0}\int_{\mathrm{D}}^{\mathrm{E}}\mathrm{d}x\,\frac{E_x}{E_{y0}+(v_\parallel/c)(BB_{x0}/B_z)}$$
$$-eE_{y0}\int_{\mathrm{D}}^{\mathrm{E}}\mathrm{d}t\,\frac{v_\parallel B_y}{B}. \tag{10}$$

The electron reflection will occur at point D at the moment when φ_{D} is quite small, $\varphi_{\mathrm{D}}\ll\varphi_{\mathrm{E}}$. In the following, therefore, we neglect φ_{D} compared with φ_{E}. When the electron moves from point D to point E, $v_\parallel$ has rather large positive values. This is the reason why v_{gx} is positive there. We note that v_{gx} can be close to zero because E_{y0} is negative and $v_\parallel$ is positive. Figure 3 graphically illustrates this. Hence, the denominator in the fourth term on the right-hand side of Eq. (10) can be quite small; thus the integral can take a large value. In other words, if v_{gx} is small, it takes a long time for the electron to reach the x position x_{E} from x_{D}. During this time, the electron can travel a long distance in the y direction by the $\mathbf{E}\times\mathbf{B}$ drift. As a result, the electron gains a great amount of energy from E_{y0}. Also, $v_\parallel$ can be quite large, being accelerated by the parallel electric field $E_\parallel$ for a long period of time.

In connection with this, we note that the following relation holds:

$$\int_{\mathrm{D}}^{\mathrm{E}}v_\parallel\mathrm{d}t\gg L_{\mathrm{DE}}, \tag{11}$$

where L_{DE} is the length along the field line from a certain point at x_{D} to x_{E}. This inequality is simply due to the fact that it takes a long time for a reflected electron to get to point E from point D. Again, Fig. 3 shows this. On the other hand, if the sign of $v_\parallel$ is reversed in Fig. 3, with the $\mathbf{E}\times\mathbf{B}$ drift velocity unchanged, then v_{gx} would become larger in magnitude. Thus we will have

$$\left|\int_{\mathrm{B}}^{\mathrm{C}}v_\parallel\mathrm{d}t\right|<L_{\mathrm{BC}}, \tag{12}$$

where L_{BC} is the length of a field line from $x=x_{\mathrm{B}}$ to $x=x_{\mathrm{C}}$. This is also the case for the integral $\int E_\parallel v_\parallel\mathrm{d}t$. From the above discussion, it is evident that

$$\left|\int_{\mathrm{D}}^{\mathrm{E}}E_\parallel v_\parallel\mathrm{d}t\right|\gg\left|\int_{\mathrm{B}}^{\mathrm{C}}E_\parallel v_\parallel\mathrm{d}t\right|, \tag{13}$$

if $E_\parallel$ in $x_{\mathrm{D}}<x<x_{\mathrm{E}}$ and $E_\parallel$ in $x_{\mathrm{C}}<x<x_{\mathrm{B}}$ are of the same order of magnitude. Consequently, $v_\parallel^2$ and hence $v_\parallel$ can be large when the particle reaches point E from point D.

Now we can show that the change in the particle energy along the trajectory B→C→D is much smaller in magnitude than the energy increase along D→E,

$$|K_{\mathrm{DE}}|\gg|K_{\mathrm{BC}}|,|K_{\mathrm{CD}}|. \tag{14}$$

Using the above discussion, we can prove this analytically (see the Appendix). Also, we can confirm this later by simulations (see Fig. 5 below). Physically, the magnitude of K_{BC} is small because the change in the energy due to the potential difference and that due to E_{y0} almost cancel, $e\varphi(x_{\mathrm{C}})-e\varphi(x_{\mathrm{B}})-eE_{y0}(y_{\mathrm{C}}-y_{\mathrm{B}})\sim 0$; they have opposite signs, even though their magnitudes are large. This is also the case when the particle moves from point C to point D. However, when it moves from point D to point E, both $e\varphi(x_{\mathrm{E}})-e\varphi(x_{\mathrm{D}})$ and $-eE_{y0}(y_{\mathrm{E}}-y_{\mathrm{D}})$ have positive values. Their sum can therefore be quite large. The fact that the length $(y_{\mathrm{E}}-y_{\mathrm{D}})$ can be large further enhances the energy.

We neglect the last term in Eq. (10) as well as K_{BC} and K_{CD}, because, as can be seen in Fig. 4, B_y is small especially behind the point x_m.

We then have the increase in the kinetic energy as

$$K_{\mathrm{BE}}=e\varphi_{\mathrm{E}}+eE_{y0}\int_{\mathrm{D}}^{\mathrm{E}}\mathrm{d}x\,\frac{E_x}{E_{y0}+(v_\parallel/c)(BB_{x0}/B_z)}. \tag{15}$$

The energy increase is due to the electric potential and the constant electric field E_{y0}. The increase by E_{y0} is enhanced by the fact that the magnitude of v_{gx} can be quite small.

To further simplify the expression for K_{BE}, we consider a case of large-amplitude wave. In the shock region, especially around the point $x=x_m$, B_z has large values, while B_y is nearly zero. We can therefore assume that

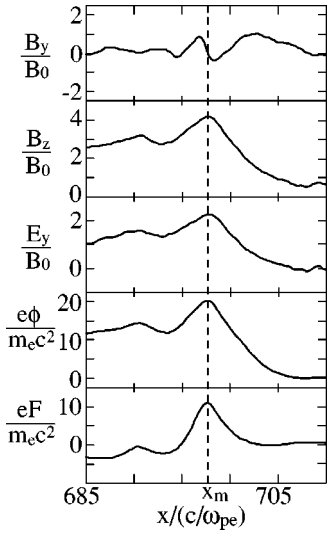

FIG. 4. Snapshots of field profiles at $\omega_{pe}t=850$.

$$B/B_z \sim 1. \tag{16}$$

Also, since $v_\parallel$ is large along the path D→E, we assume that

$$v_\parallel \sim c. \tag{17}$$

This can be valid when the amplitude is large and the external magnetic field is rather strong, $\omega_{ce} \gtrsim \omega_{pe}$; either of the two effects acts to increase the electric potential.[34,35,45–50] Furthermore, (13) indicates that $v_\parallel$ can be particularly large when the electron moves from point D to E. Then, the denominator in Eq. (15) can be approximated as

$$E_{y0}+(v_\parallel/c)(BB_{x0}/B_z) \sim E_{y0}+B_{x0}. \tag{18}$$

Integrating Eq. (15) and substituting Eq. (6) for E_{y0}, we obtain a simple expression for $K_{\rm BE}$ in the wave frame,

$$K_{\rm BE}=\frac{e\varphi_{\rm E}}{1-(v_{\rm sh}/c)(B_{z0}/B_{x0})}. \tag{19}$$

The potential $\varphi_{\rm E}$ is the maximum value of φ. This indicates that $K_{\rm BE}$ can have extremely great values when

$$1-(v_{\rm sh}/c)(B_{z0}/B_{x0}) \sim 0. \tag{20}$$

We can estimate $K_{\rm BE}$ if we know the magnitude of the potential formed in the shock wave. For a solitary pulse propagating perpendicular to a magnetic field, the potential is given as

$$e\varphi=2m_iv_{\rm A}^2(M-1), \tag{21}$$

where M is the Alfvén Mach number. This relation is valid for $1<M<2$ and for $\omega_{ce}/\omega_{pe} \lesssim 1$; we need the latter condition for the charge neutrality,[50] which is assumed in the conventional theory for the nonlinear magnetosonic wave. In Refs. 34 and 35, an expression for the magnitude of the potential, which is applicable to cases with $M>2$ or $\omega_{ce}/\omega_{pe}>1$, was derived as

$$e\varphi=\frac{B_0(B-B_0)}{4\pi n_0}, \tag{22}$$

in the wave frame. In this theory, the magnetic field has only the z component (perpendicular propagation). The maximum value of B is given as

$$\frac{B}{B_0}=\left(1+\frac{m_i\gamma_{\rm sh}n_0v_{\rm sh}^2}{(B_0^2/8\pi)}\right)^{1/2}, \tag{23}$$

where $\gamma_{\rm sh}=(1-v_{\rm sh}^2/c^2)^{-1/2}$.

Even in oblique shock waves, B_z becomes the dominant component of **B** if the wave amplitude is large. We may therefore use Eq. (22) for the estimate of $K_{\rm BE}$. (For the potential in a small-amplitude oblique magnetosonic wave, see Ref. 46.)

III. REFLECTION AND TRAPPING

Some electrons can be reflected near the end of the main pulse when, roughly speaking, a potential dip is formed there. More precisely, the reflection can take place when the quantity F becomes small there.[43] For a stationary state, F is defined as

$$F=-\int\frac{(\mathbf{E}\cdot\mathbf{B})}{B}{\rm d}s=-\int\frac{(E_xB_{x0}+E_{y0}B_y)}{B}\frac{B}{B_{x0}}{\rm d}x, \tag{24}$$

where ds is the length along the field line,

$${\rm d}s=(B/B_{x0})v_{gx}{\rm d}t. \tag{25}$$

The quantity F has a similar profile to φ and B_z. The reflected electrons then begin oscillatory motion in the main pulse region, i.e., motions like D→E→B→C→D in Fig. 2. When they return to point D (or near D), they will again be reflected forward. This second reflection occurs even when the values of F around point D have already been recovered by this time and are not small anymore. We discuss this second reflection mechanism here. (The first reflection was studied in detail in Ref. 43.)

At the moment of electron reflection, the electron energies are not very high. The strong acceleration takes place after the reflection. For simplicity, therefore, we use a nonrelativistic theory. From the equation of motion for electrons, we have the following equation in the wave frame,[43]

$$\begin{aligned}(m_e/2)(v_\parallel-v_{\rm rv})^2=e(F-F_0)-K-\mu(B-B_0)+(m_e/2)&\\ \times(v_{\parallel0}^2+v_{d0}^2)-m_ec(E_{y0}/B_{x0})&\\ \times(v_{dz}-v_{z0})-(m_e/2)v_d^2,&\end{aligned} \tag{26}$$

where $v_{\rm rv}$ and K are defined as

$$v_{\rm rv}=-cE_{y0}B_z/(B_{x0}B) \quad (>0), \tag{27}$$

$$K=-m_ev_{\rm rv}^2/2 \quad (<0), \tag{28}$$

and μ is the magnetic moment,

$$\mu=m_ev_\perp^2/(2B), \tag{29}$$

with $v_\perp$ the gyration speed perpendicular to the magnetic field.

As Eq. (5) indicates, the fluid parallel velocity is negative in the far upstream region; $\langle v_{\parallel0}\rangle=-v_{\rm sh}\cos\theta$. We thus consider here an electron particle penetrating the shock re-

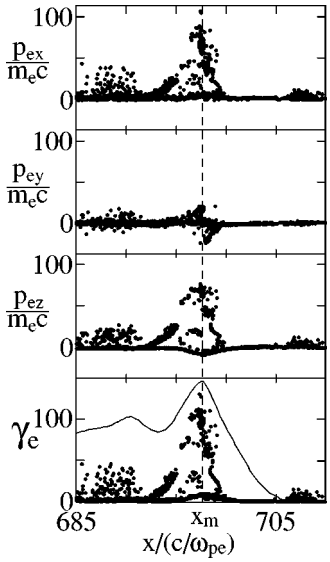

FIG. 5. Phase space plots of electrons.

gion with a negative parallel velocity. (Particles can have positive parallel velocities. If $v_\parallel$ is too large, however, v_{gx} cannot be negative.) The particle will not be able to enter a region where the right-hand side of Eq. (26) has negative values. If such a region appears, the particle will be reflected; if we neglect unimportant terms, we can say that the reflection takes place when $[e(F-F_0)-K]$ becomes negative near the end of the pulse. (The reflection will not occur around the point $x=x_m$, because φ and hence F are large there.) The reflection occurs when the velocity v_{gx} is reversed, from negative to positive. Equation (2) shows that v_{gx} changes its sign when $v_\parallel=v_{\rm rv}$. That is, the parallel velocity has already changed to positive values before the reflection. After the reflection, $v_\parallel$ further increases until the particle reaches the point $x=x_m$ and then decreases, because the parallel electric field changes the sign as one moves as D→E→B. The particle will then be reflected backward near the leading edge of the main pulse. Simulations indicate that this point, which will be designated by $x_{\rm B2}$, is in the pulse region, $x_m<x_{\rm B2}<x_{\rm B}$ (see Fig. 5). It thus follows that $F(x_m)>F(x_{\rm B2})>F(x_{\rm B})=F_0$.

We now show that the particle will be reflected forward again near the end of the pulse, $x\sim x_{\rm D}$, even if the values of F near there are not so small at this time. We denote the time when the particle arrives at point B from the upstream region for the first time by $t_{\rm B1}$. After being reflected at $x=x_{\rm D}$ ($t=t_{\rm D1}$), it will arrive at $x_{\rm B2}$ at time $t=t_{\rm B2}$. We assume that during the time from $t=t_{\rm D1}$ to $t=t_{\rm B2}$, the field values change slightly around $x=x_{\rm D}$ so that $F(x_{\rm D})$ is not small anymore at $t=t_{\rm B2}$. If the wave is stationary after $t=t_{\rm B2}$, then we can apply Eq. (26) to this particle for $t\geqslant t_{\rm B2}$,

$$(m_e/2)(v_\parallel-v_{\rm rv})^2=e(F-F_2)-K-\mu(B-B_2)+(m_e/2)\times(v_{\parallel 2}^2+v_{d2}^2)-m_e c(E_{y0}/B_{x0})\times(v_{dz}-v_{z2})-(m_e/2)v_d^2, \quad (30)$$

where the subscript 2 refers to the values at the particle position $x_{\rm B2}$, i.e., $F_2=F(x_{\rm B2})$. At $t=t_{\rm B2}$, $v_\parallel$ is equal to $v_{\rm rv}$; because $v_{gx}=0$. The left-hand side of Eq. (30) is therefore equal to zero at this moment.

At $t=t_{\rm B1}$, when the particle penetrated the shock region for the first time, $v_\parallel$ was negative and the value of Eq. (26) was positive. [More generally, unless $v_\parallel$ is equal to $v_{\rm rv}$, Eq. (26) is positive.] The situation is thus quite different at $t=t_{\rm B2}$. At this moment, the right-hand side of Eq. (30) is zero. Hence, the particle will be confined in the region $e(F-F_2)-K\gtrsim 0$. Since F_2 is greater than F_0, a dip of F is not needed for the second reflection near the end of the main pulse (near point D).

Once an electron is reflected, then it can hardly escape from the shock wave. The number of trapped electrons thus continues to increase as a shock wave propagates; when F becomes small near the end of the pulse, electrons that happen to be there will be newly trapped.

IV. SIMULATION RESULTS

To investigate electron acceleration in oblique magnetosonic shock waves in more detail, we have performed numerical simulations using a one-dimensional (one spatial coordinate and three velocity components), relativistic, electromagnetic, particle simulation code with full ion and electron dynamics.[51] Since the simulation methods for the study of shock waves were described in Refs. 30, 43, 44, we do not go into details of the methods.

Here, we have used the following simulation parameters. The total system length is $L=4{,}096\Delta_g$, where Δ_g is the grid spacing; the numbers of ions and electrons are $N_i=N_e=262{,}144$; the mass ratio is $m_i/m_e=100$; the propagation angle is $\theta=45°$; the ratio of the electron cyclotron frequency to the electron plasma frequency is $\omega_{ce}/\omega_{pe}=3.0$ in the upstream region; the light speed is $c/(\omega_{pe}\Delta_g)=4.0$; and the electron and ion thermal velocities in the upstream region are $v_{T_e}/(\omega_{pe}\Delta_g)=0.4$ and $v_{T_i}/(\omega_{pe}\Delta_g)=0.04$, respectively. The Alfvén speed is then $v_{\rm A}/(\omega_{pe}\Delta_g)=1.2$. The time step is $\omega_{pe}\Delta t=0.02$. In this section, all the simulation results are shown in the laboratory frame.

Figure 4 shows field profiles in a shock wave propagating in the x direction with a speed $v_{\rm sh}=2.2v_{\rm A}$. From the top panel to the bottom one, plotted are the y component of the magnetic field B_y, the z component B_z, the y component of the electric field E_y, electric potential φ, and F. We obtained φ and F using the following equations:

$$\varphi=-\int^x E_x {\rm d}x, \quad (31)$$

$$F=-\int^x E_\parallel \frac{B}{B_x}{\rm d}x. \quad (32)$$

The x component of the electric field is given as $E_x=-\partial\varphi/\partial x$, and B_x is constant. The quantity E_z, which is not shown here and is rather weak compared with E_x or E_y, has a profile similar to $-E_x$. The quantities B_z, E_y, φ, and F take their maximum values at nearly the same position, $x=x_m$, which is denoted by the dotted line in the figure, while $B_y\sim 0$ around this point. These properties are consis-

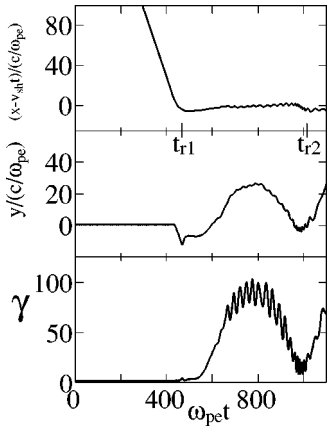

FIG. 6. Time variations of $(x-v_{\rm sh}t)$, y, and γ of a reflected electron.

tent with the assumptions made in the theory. In this snapshot at $\omega_{pe}t=850$, values of F near the end of the main pulse, $x/(c/\omega_{pe})\sim 693$, are smaller than those in the upstream region. Thus, electrons can be reflected there at this moment.

We show in Fig. 5 phase space plots of electrons at $\omega_{pe}t=850$; (x,p_{ex}), (x,p_{ey}), (x,p_{ez}), and (x,γ_e). In the bottom panel, we have also shown the profile of φ to compare with the plot of (x,γ_e). The dotted line represents the position $x=x_m$. The electrons reflected near the end of the main pulse have their maximum energies, $\gamma_e\sim 130$ in this case, near the point $x=x_m$. Energies of passing electrons remain low.

Figure 6 shows time variations of $(x-v_{\rm sh}t)$, y, and γ of a reflected electron; we have chosen a typical reflected electron and followed its trajectory. In the top panel, the position $x-v_{\rm sh}t=0$ refers to the position $x=x_m$; the value of $v_{\rm sh}$ used here is the shock speed time averaged over t_{r1} to t_{r2}. This electron is reflected at time $t=t_{r1}$. After this time, the quantity $(x-v_{\rm sh}t)$ dose not decrease, and γ starts to increase, having its maximum value at $\omega_{pe}t\sim 780$. At $t=t_{r2}$, the second reflection near the end of the pulse occurs. In addition to this long period oscillation, we observe a short period oscillation, with period $\omega_{pe}t\sim 30$ around the time $\omega_{pe}t=780$. This oscillation is due to the cyclotron motion.

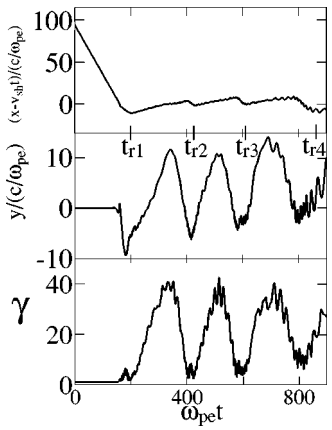

FIG. 7. Time variations of $(x-v_{\rm sh}t)$, y, and γ of a reflected electron in a weaker shock wave.

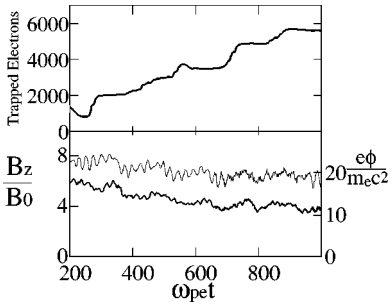

FIG. 8. Time variations of the number of trapped electrons (upper panel) and the maximum values of φ and B_z (lower panel). The shock propagation speed is $v_{\rm sh}=2.2v_{\rm A}$.

The period of the slow oscillatory motion of trapped electrons, as well as the cyclotron period, decreases with decreasing electron energy. Hence, to observe the oscillatory motion more clearly, we have carried out a simulation of a weaker shock wave. Figure 7 shows the same quantities, $(x-v_{\rm sh}t)$, y, and γ, of a reflected electron in a weaker shock wave with $v_{\rm sh}=1.8v_{\rm A}$. In this weaker shock wave, the maximum electron energy is lower, $\gamma\sim 40$. The periods of the long and short period oscillations are, respectively, shorter than those in Fig. 6. We observe in Fig. 7 that the electron is reflected four times in the end of the main pulse region at times $t=t_{r1}$, t_{r2}, t_{r3}, and t_{r4} by the end of the simulation.

The expression for v_{gx}, Eq. (2), explains the tendency that the period of the oscillation rises with the shock strength. The magnitude of v_{gx} decreases as the amplitude of the shock wave is increased, because B_{x0}/B decreases more than $|E_{y0}|B_z/B^2$ with the amplitude. Hence, the second term $(v_\parallel B_{x0}/B)$ on the right-hand side of Eq. (2) cannot greatly exceed the first term when the amplitude is large.

Once electrons are reflected, they are then trapped. Hence, the number of trapped electrons would increase. The upper panels in Figs. 8 and 9 show this. Here, we counted the high-energy electrons ($\gamma\geqslant 20$ for Fig. 8 and $\gamma\geqslant 15$ for Fig. 9) in the region $|x-x_m|\leqslant 25(c/\omega_{pe})$. Also, low-energy electrons in this region were counted if they had been reflected near the end of the main pulse before. Figures 8 and 9 show, respectively, the cases with $v_{\rm sh}=2.2v_{\rm A}$ and with $v_{\rm sh}=1.8v_{\rm A}$. In either case, the number of trapped electrons increases with time. The lower panels show time variations of the maximum values of the potential (thin line) and of B_z

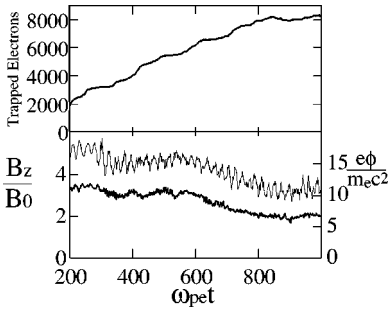

FIG. 9. Time variations of the number of trapped electrons (upper panel) and the maximum values of φ and B_z (lower panel). The shock propagation speed is $v_{\rm sh}=1.8v_{\rm A}$.

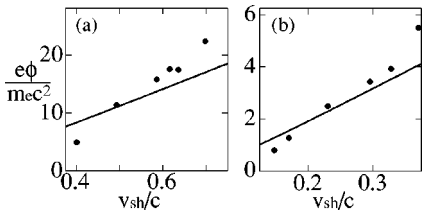

FIG. 10. Potential vs shock propagation speed v_{sh}. Here, $\omega_{ce}/\omega_{pe}=3.0$ and $\theta=45°$ in (a), while $\omega_{ce}/\omega_{pe}=1.0$ and $\theta=66°$ in (b).

(thick line). In these figures, the wave amplitudes are gradually decreasing with time, owing to energy dissipation. However, the numbers of trapped electrons are increasing.

Figure 10 shows the maximum value of φ as a function of the shock propagation speed v_{sh}; the dots and solid lines represent simulation and theoretical values, respectively. Figure 10(a) shows the case with $\omega_{ce}/\omega_{pe}=3.0$ and $\theta=45°$, while Fig. 10(b) shows the case with $\omega_{ce}/\omega_{pe}=1.0$ and $\theta=66°$. The potential was measured at $\omega_{pe}t=600$ in the simulations. The shock propagation speed v_{sh} was changed by changing the shock strength. Even though we used the theory for perpendicular waves,[35] the theoretical estimates agree fairly well with the simulation results.

Figure 11 shows the maximum electron energy, γ_m, as a function of v_{sh}. The simulation parameters in Figs. 11(a) and 11(b) are the same as the ones in Figs. 10(a) and 10(b), respectively. The dots and solid lines represent simulation and theoretical values, respectively. For comparison, we also show, by dashed lines, the theoretical values obtained in the previous paper, Ref. 44. The old theory does not give real values for $v_{sh}/c<0.46$ for the parameters in Fig. 11(a) and for $v_{sh}/c<0.13$ in Fig. 11(b). Even though the theory developed in this paper is much simpler, it gives real values of γ_m for any v_{sh} and agrees well with the simulation results.

V. SUMMARY

We have theoretically and numerically studied the electron acceleration to ultrarelativistic energies by a shock wave propagating obliquely to a magnetic field. Electrons can be reflected near the end of the main pulse region of the shock wave when the potential φ (or more precisely, F) happens to be small there. They are then trapped in the main pulse region. Their energies take their maximum values at the position of the maximum electric potential, $x=x_m$.

Using the energy conservation equation and drift approximation in the wave frame, we theoretically obtained the maximum energy of reflected electrons. The derivation and final expression are much simpler than those in the previous paper.[44] Furthermore, we discussed the physical meaning of the calculations in detail. The reflected electrons gain energy from the electric potential and the constant electric field $E_{y0}(<0)$; $e\varphi-eE_{y0}\int v_y dt$. When the reflected electrons move from the reflection point to the point $x=x_m$, the guiding center velocity v_{gx} can be quite small; thus it can take long periods of time for these electrons to reach the point x_m. Therefore, $\int v_y dt$ can be large, and the reflected electrons can gain a great amount of energy from the electric field E_{y0}. In addition, we have pointed out that once some electrons are reflected, they can hardly be detrapped; even after the negative potential dip φ (or F) disappeared. This suggests that the number of trapped electrons continually grows.

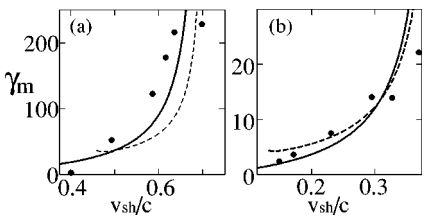

FIG. 11. The maximum electron energy γ_m as a function of v_{sh}. The simulation parameters are the same as those in the previous figure.

We then studied the electron acceleration and shock propagation with a one-dimensional, relativistic, electromagnetic particle simulation code with full ion and electron dynamics. Trajectories of reflected electrons in a shock wave were examined. We showed that the theoretical expressions for the potential and the maximum electron energy are in fairly good agreement with the simulation result. Also, we observed that the number of trapped electrons increases with time.

ACKNOWLEDGMENTS

This work was carried out by the joint research program of the Solar-Terrestrial Environment Laboratory, Nagoya University, and was supported in part by the Grant-in-Aid for Scientific Research from the Japan Society for the Promotion of Science.

APPENDIX: MAGNITUDES OF K_{BC}, K_{DE}, AND $E_{\parallel}$

The energy change K_{BC} is calculated as

$$K_{BC}=-e\int_B^C (E_x v_x+E_{y0}v_y)\mathrm{d}t. \tag{A1}$$

Substituting Eqs. (2) and (3) for v_x and v_y yields

$$K_{BC}=-e\int_B^C \frac{v_\parallel}{B}(E_x B_{x0}+E_{y0}B_y)\mathrm{d}t. \tag{A2}$$

We have similar equations for K_{CD} and K_{DE}. This expression clearly shows that K_{DE} can be large, because $v_\parallel$ can be large and the time is long when the particle moves from point D to point E.

We now estimate the magnitude of $\mathbf{E}\cdot\mathbf{B}$. In ideal magnetohydrodynamics, the electric field parallel to the magnetic field is zero,

$$\mathbf{E}\cdot\mathbf{B}=0. \tag{A3}$$

On the other hand, in a two-fluid model, perturbations E_{x1} and E_{z1} in a small-amplitude oblique magnetosonic wave with a propagation angle θ are given as

$$E_{x1}=-\frac{m_i}{e}\left[\frac{v_{p0}^2(v_{p0}^2-c_s^2)}{v_{p0}^2-v_A^2\cos^2\theta}+\frac{\Gamma_e T_e}{m_i}\right]\frac{1}{n_0}\frac{\partial n_1}{\partial x}, \tag{A4}$$

$$E_{z1}=\frac{m_i}{e}\frac{v_{p0}^2(v_{p0}^2-c_s^2)}{(v_{p0}^2-v_{\mathrm{A}}^2\cos^2\theta)}\frac{\cot\theta}{n_0}\frac{\partial n_1}{\partial x}, \tag{A5}$$

in the laboratory frame.[46] Here, Γ_e is the specific heat ratio of electrons, and c_s is the sound speed, $c_s^2=(\Gamma_e p_{e0}+\Gamma_i p_{i0})/(n_0 m_i)$ with p_{j0} ($j=e$ or i) the equilibrium pressure. Accordingly, $\mathbf{E}\cdot\mathbf{B}$ is calculated as

$$\mathbf{E}\cdot\mathbf{B}=-\frac{\Gamma_e T_e}{e}\frac{B_{x0}}{n_0}\frac{\partial n_1}{\partial x}. \tag{A6}$$

Here, we have neglected second order terms such as $E_{y1}B_{y1}$.

We have obtained (A6) using the quantities in the laboratory frame. It is noted, however, that the value of $\mathbf{E}\cdot\mathbf{B}$ is invariant against Lorentz transformation.

Furthermore, in a large-amplitude wave, $\mathbf{E}\cdot\mathbf{B}$ can be even larger than Eq. (A6).[43,44]

[1] S. R. Kane, K. Kai, T. Kosugi, S. Enome, P. B. Landecker, and D. L. McKenzie, Astrophys. J. **271**, 376 (1983).
[2] D. J. Forrest and E. L. Chupp, Nature (London) **305**, 291 (1983).
[3] H. Nakajima, T. Kosugi, K. Kai, and S. Enome, Nature (London) **305**, 292 (1983).
[4] S. R. Kane, E. L. Chupp, D. J. Forrest, G. H. Share, and E. Rieger, Astrophys. J. Lett. **300**, L95 (1986).
[5] E. L. Chupp, H. Debrunner, E. Flückiger *et al.*, Astrophys. J. **318**, 913 (1987).
[6] K. Koyama, R. Petre, E. V. Gotthelf *et al.*, Nature (London) **378**, 255 (1995).
[7] T. Tanimori, Y. Hayami, S. Kamei *et al.*, Astrophys. J. Lett. **497**, L25 (1998).
[8] T. Tanimori, K. Sakurazawa, S. A. Dazeley *et al.*, Astrophys. J. Lett. **492**, L33 (1998).
[9] F. A. Aharonian, A. G. Akhperjanian, J. A. Barrio *et al.*, Astrophys. J. **539**, 317 (2000).
[10] D. A. Leahy, F. A. Harrison, and A. Yoshida, Astrophys. J. **475**, 823 (1997).
[11] F. A. Harrison, P. S. Ray, D. A. Leahy *et al.*, Astrophys. J. **528**, 454 (2000).
[12] E. Pian, G. Vacanti, G. Tagliaferri *et al.*, Astrophys. J. Lett. **492**, L17 (1998).
[13] J. Kataoka, J. R. Mattox, J. Quinn *et al.*, Astrophys. J. **514**, 138 (1999).
[14] G. M. Madejski, M. Sikora, T. Jaffe *et al.*, Astrophys. J. **521**, 145 (1999).
[15] L. Maraschi, G. Fossati, F. Tavecchio *et al.*, Astrophys. J. Lett. **526**, L81 (1999).
[16] D. Petry, M. Böttcher, V. Connaughton *et al.*, Astrophys. J. **536**, 742 (2000).
[17] E. Fermi, Phys. Rev. **75**, 1169 (1949).
[18] R. D. Blandford and D. Eichler, Phys. Rep. **154**, 1 (1987).
[19] S. P. Reynolds and D. C. Ellison, Astrophys. J. Lett. **399**, L75 (1992).
[20] J. E. Gunn and J. P. Ostriker, Phys. Rev. Lett. **22**, 728 (1969).
[21] C. S. Wu, J. Geophys. Res. **89**, 8857 (1984).
[22] M. M. Leroy and A. Mangeney, Ann. Geophys. (France) **2**, 449 (1984).
[23] M. E. Dieckmann, K. G. McClements, S. C. Chapman, R. O. Dendy, and L. O'C. Drury, Astron. Astrophys. **356**, 377 (2000); Phys. Plasmas **5**, 3257 (1998).
[24] T. P. Armstrong, G. Chen, E. T. Sarris, and S. M. Krimigis, in *Study of Traveling Interplanetary Phenomena*, edited by M. A. Shea and D. F. Smart (Reidel, Dordrecht, 1977), p. 367.
[25] R. B. Decker, Space Sci. Rev. **48**, 195 (1988).
[26] C. Joshi, C. E. Clayton, W. B. Mori, J. M. Dawson, and T. Katsouleas, Colloids Surf., A **16**, 65 (1994).
[27] D. Biskamp and H. Welter, Nucl. Fusion **12**, 663 (1972).
[28] M. M. Leroy, D. K. Winske, C. C. Goodrich, C. S. Wu, and K. Papadopoulos, J. Geophys. Res. **87**, 5081 (1982).
[29] D. W. Forslund, K. B. Quest, J. U. Brackbill, and K. Lee, J. Geophys. Res. **89**, 2142 (1984).
[30] Y. Ohsawa, Phys. Fluids **28**, 2130 (1985).
[31] Y. Ohsawa, J. Phys. Soc. Jpn. **55**, 1047 (1986).
[32] R. L. Tokar, S. P. Gary, and K. B. Quest, Phys. Fluids **30**, 2569 (1987).
[33] B. Lembege and J. M. Dawson, Phys. Fluids B **1**, 1001 (1989).
[34] S. Nakazawa and Y. Ohsawa, J. Phys. Soc. Jpn. **66**, 2044 (1997).
[35] S. Nakazawa and Y. Ohsawa, J. Phys. Soc. Jpn. **66**, 2965 (1997).
[36] S. Nakazawa and Y. Ohsawa, J. Phys. Soc. Jpn. **67**, 176 (1998).
[37] K. Maruyama, N. Bessho, and Y. Ohsawa, Phys. Plasmas **5**, 3257 (1998).
[38] T. Masaki, H. Hasegawa, and Y. Ohsawa, Phys. Plasmas **7**, 529 (2000).
[39] S. Usami and Y. Ohsawa, Phys. Plasmas **8**, 2666 (2001).
[40] M. Toida and Y. Ohsawa, J. Phys. Soc. Jpn. **64**, 2038 (1995).
[41] M. Toida and Y. Ohsawa, Sol. Phys. **171**, 161 (1997).
[42] N. Bessho, K. Maruyama, and Y. Ohsawa, J. Phys. Soc. Jpn. **68**, 1 (1999).
[43] N. Bessho and Y. Ohsawa, Phys. Plasmas **6**, 3076 (1999).
[44] N. Bessho and Y. Ohsawa, Phys. Plasmas **7**, 4004 (2000).
[45] T. Kakutani, H. Ono, T. Taniuti, and C. C. Wei, J. Phys. Soc. Jpn. **24**, 1159 (1968).
[46] Y. Ohsawa, Phys. Fluids **29**, 1844 (1986).
[47] J. H. Adlam and J. E. Allen, Philos. Mag. **3**, 448 (1958).
[48] L. Davis, R. Lüst, and A. Schlüter, Z. Naturforsch. A **13A**, 916 (1958).
[49] C. S. Gardner and G. K. Morikawa, Commun. Pure Appl. Math. **18**, 35 (1965).
[50] Y. Ohsawa, Phys. Fluids **29**, 2474 (1986).
[51] P. C. Liewer, A. T. Lin, J. M. Dawson, and M. Z. Caponi, Phys. Fluids **24**, 1364 (1981).